

# Journal of Photonics for Energy

SPIEDigitalLibrary.org/jpe

## ***Ab initio* modeling of water–semiconductor interfaces for photocatalytic water splitting: role of surface oxygen and hydroxyl**

Brandon C. Wood  
Tadashi Ogitsu  
Eric Schwegler

# ***Ab initio* modeling of water–semiconductor interfaces for photocatalytic water splitting: role of surface oxygen and hydroxyl**

**Brandon C. Wood, Tadashi Ogitsu, and Eric Schwegler**

Lawrence Livermore National Laboratory, Quantum Simulations Group, 7000 East Avenue,  
Livermore, California 94550  
[wood37@llnl.gov](mailto:wood37@llnl.gov)

**Abstract.** We perform extensive density-functional theory total-energy calculations and *ab initio* molecular-dynamics simulations to evaluate the structure, stability, and reactivity of oxygen- and hydroxyl-decorated InP(001) surfaces for photoelectrochemical water cleavage. Surface oxygen is adsorbed in one of two primary local bond topologies: In–O–P and In–O–In. We show that the chemical activity of the oxygen-decorated surface toward water dissociation can be connected to the local oxygen bond topology, with In–O–In bridges promoting spontaneous water dissociation. Surface hydroxyl groups tend to form either In–OH–In bridges, though the second of the two In–OH bonds is easily broken. Dynamics simulations of the full water–semiconductor interface show surface proton transfer when the surface is hydroxylated, facilitated by strong hydrogen bonding between atop OH groups and with interfacial water molecules. Implications for understanding the reaction dynamics at InP(001)–water interfaces are discussed. © 2011 Society of Photo-Optical Instrumentation Engineers (SPIE). [DOI: [10.1117/1.3625563](https://doi.org/10.1117/1.3625563)]

**Keywords:** photoelectrochemical; hydrogen production; III-V semiconductors; indium phosphide.

Paper 11181PR received Feb. 8, 2011; revised manuscript received May 19, 2011; accepted for publication Jul. 26, 2011; published online Aug. 29, 2011.

## **1 Introduction**

Development of efficient, environmentally responsible processes for the production of chemical fuel using sunlight has been identified by the U.S. Department of Energy as a strategic goal for a secure and sustainable energy future.<sup>1</sup> Semiconductor-based photoelectrochemical (PEC) hydrogen production from water is particularly attractive, thanks to a simple device design and the promise of efficient photon harvesting.<sup>2–4</sup> Nevertheless, practical implementations of PEC devices have been limited, in part, because the relevant chemical processes at the electrode–water interface are poorly understood.

A schematic illustration of a *p*-type semiconductor-based PEC cell is given in Fig. 1. In this model, the semiconductor serves a dual function as a photon harvester and catalytic surface for hydrogen evolution from water.<sup>1,3</sup> For maximum effectiveness, a PEC semiconductor photocatalyst should have a bandgap that is optimized to the solar spectrum, with valence- and conduction-band edges that closely match the redox potentials of water, which may themselves be modulated by electrolytes or surface states. Recognizing this, past efforts have concentrated on engineering the bandgap and level alignment to the redox potential of water. However, high solar-to-fuel conversion efficiency has generally come at the expense of short device lifetime due to fast degradation of the electrode.<sup>5–8</sup>

It has been suggested that oxygen, which is present in high concentrations as a contaminant on (001) surfaces of III-V semiconductors, may play a significant role in both the surface

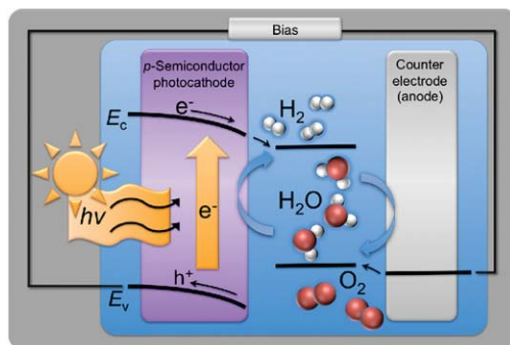


**Fig. 1** Schematic of a simple PEC device based on a  $p$ -type photocathode. Photoexcitation occurs in the semiconductor photocathode, which is immersed with a counter-electrode in an open-circuit configuration in a water-based liquid electrolyte. The valence and conduction band edges, which sandwich the redox potentials of water, bend near the interface to facilitate electron-hole separation. Catalytic evolution of hydrogen occurs at the semiconductor–water interface.

photocorrosion and the photocatalytic water-splitting reactions.<sup>8–11</sup> Given the apparent connection between high catalytic activity and the potential for surface degradation in III-V systems, evaluating this potential role of oxygen represents a high priority for developing a complete understanding of PEC device shortcomings under real-world operating conditions. Nevertheless, although the water–InP(001) interface has been investigated theoretically<sup>12</sup> the role of surface oxygen has not been explored in detail.

Here we use a combination of *ab initio* molecular dynamics simulations and total-energy calculations based on density functional theory (DFT) to understand the chemistry of a model electrode/electrolyte interface consisting of oxygen- and hydroxyl-rich InP(001) surfaces and water. The choice of InP(001) is motivated by its known water-splitting activity (although its band gap of 1.35 eV is slightly too small for use in a practical PEC device).<sup>13</sup> Our results are used to explore the effect of oxide and hydroxide surface morphologies on surface stability and reactivity, and to evaluate the specific role of interfacial water and surface dynamics in the relevant chemical processes.

## 2 Methods

Results are based on density functional theory within the plane-wave pseudopotential formalism, as calculated using the Quantum-ESPRESSO code.<sup>14</sup> The Perdew–Burke–Ernzerhof (PBE) exchange-correlation functional was used.<sup>15</sup> Ultrasoft pseudopotentials<sup>16</sup> were used for all elements, and semicore  $d$  states were included in the electronic valence description for indium. For the total-energy ionic relaxation calculations, five-layer InP(001) slabs were used to ensure both exposed surfaces were In-rich, thereby minimizing spurious interactions between periodic slab images. The bottom two layers were fixed to the bulk geometry, with all remaining atoms free to move. A vacuum separation of 12 Å was inserted between periodic slab images.

Molecular-dynamics results were obtained within the Car–Parrinello framework,<sup>17</sup> using D<sub>2</sub>O in lieu of H<sub>2</sub>O to permit larger time steps. The fictitious electronic mass was chosen as 700 a.u., using a time step of 12 a.u. All simulations were run within the canonical  $NVT$  ensemble, with temperatures maintained using Nose–Hoover chains.<sup>18</sup> Simulations were run at 400 K in order to properly reproduce the structural properties of liquid water.<sup>19</sup> A weak thermostat was also added to the electronic degrees of freedom in order to maintain separation from the ionic degrees of freedom over long simulation trajectories.

For simulations of the full semiconductor–water surface, seven semiconductor layers were included in a surface slab configuration, with 16 atoms per layer (112 semiconductor atoms, excluding the surface oxygen/hydroxyl atoms). All exposed surfaces were indium-rich InP(001).

In-plane axes were aligned along the  $[110]$  and  $[\bar{1}10]$  crystallographic directions. A total of 142 water molecules were inserted between periodic slab images, filling an intermediate region of 16.5 Å wide (the density was chosen to match the experimental density of liquid water). To generate the initial configuration for the interface, we first ran classical simulations for bulk water using the TIP4P potential. The water molecules were then inserted into the full model structure, and the system was equilibrated for 1 ps with the surface degrees of freedom kept frozen. Another 3 ps of equilibration was then performed with all degrees of freedom active before the production runs, which were 15 ps each.

### 3 Structure of Oxygen-Rich Indium Phosphide (001)

Our purpose lies in evaluating the effect of surface oxygen on the structure and stability of InP(001); however, the exact structure of oxygen-rich InP(001) surfaces has been difficult to determine.<sup>7,20–24</sup> We have therefore extracted low-energy candidate configurations by adsorbing atomic oxygen on high-symmetry sites of an initially unreconstructed In-rich InP(001) surface slab, then allowing the atoms to relax into their local-minimum configuration. Atop, hollow, and both bridge sites were tested in the high coverage (1.0 ML) limit, with four surface adsorbate atoms decorating a  $(2 \times 2)$  supercell (see Fig. 2 for schematic of initial adsorption sites). Site symmetry was broken by displacing the four oxygen atoms off their ideal sites in symmetric and antisymmetric patterned configurations.

This procedure exposed seven total morphologies, which are shown in Fig. 3. The corresponding formation energies are given in Table 1 with respect to two reference configurations. The first is with respect to molecular  $O_2$ , whereas the second is with respect to  $H_2O$  and  $H_2$ . For the InP(001) reference phase, we used the  $\delta(2 \times 4)$  mixed-dimer reconstruction, which is the most commonly observed In-rich reconstruction in vacuum.<sup>25,26</sup> It is worth emphasizing that the symmetry sites listed in Table 1 represent initial oxygen adsorption sites, which may not necessarily resemble the final configurations in Fig. 3. To avoid further confusion, we index the morphologies in Table 1 with a letter corresponding to the initial adsorption site ( $A$  = atop,  $X$  = bridge  $x$ ,  $Y$  = bridge  $y$ ,  $H$  = hollow) and a numerical index to distinguish the different configurations for the  $A$  and  $H$  symmetry sites.

All tested configurations show that incorporation of oxygen is thermodynamically favored with respect to the clean surface in the presence of gaseous  $O_2$ , in agreement with experimental observations of high surface oxygen contamination under atmospheric conditions.<sup>8,9,11,27</sup> When taken with respect to water, however, incorporation is endothermic.

It is immediately evident from Fig. 3 that oxygen incorporation is characterized by two primary topological motifs: In–O–In and In–O–P. Because our (001) surface layer is heavily In-rich, the In–O–In configuration corresponds to surface oxygen, whereas the In–O–P configuration corresponds to subsurface oxygen that bridges two layers. The relative concentrations of In–O–In and In–O–P motifs are listed alongside the formation energies in Table 1. In some

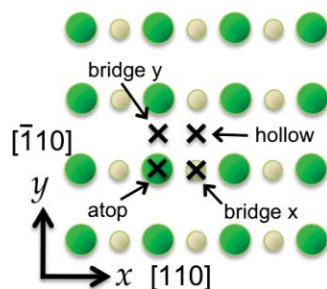


**Fig. 2** High-symmetry sites for initial adsorption on unreconstructed InP(001). Indium atoms (large, dark circles) form the surface layer, with phosphorous atoms (small, light circles) in the subsurface layer (Online color scheme: In = green, P = gold).

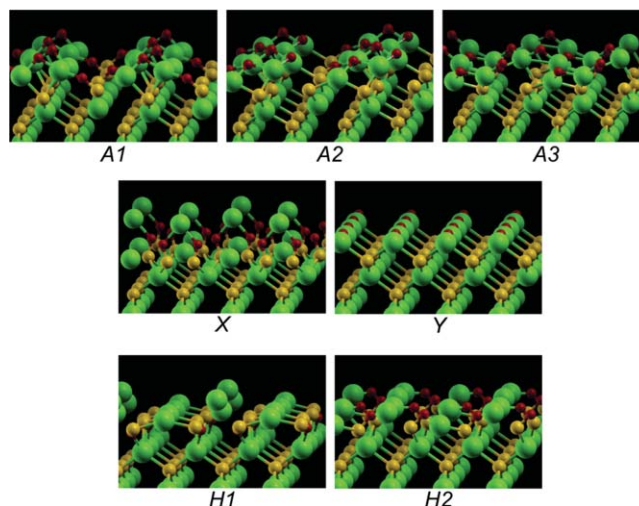


**Fig. 3** Relaxed structures for the oxygen-rich surfaces listed in Table 1. Views are along the  $[\bar{1}10]$  crystallographic direction. Large spheres are In atoms; smaller light and dark spheres are P and O atoms, respectively. (Online color scheme: In = green, P = gold, O = red).

of the structures (*X*, in particular), the oxygen pushes the indium to which it is bonded far out of the indium plane.

The *X* configuration is the most stable of those we tested, whereas *Y* is the least stable by  $\sim 1$  eV. Although this may point to a strong preference of the In–O–P bridge over the In–O–In bridge, this conclusion is tenuous, given that the three *A* configurations also contain large fractions of In–O–In bonds but, nevertheless, have relatively low formation energies. Closer examination reveals that *Y* has an unusually large bending strain induced in the In–O–In bond, which is a consequence of forced simultaneous occupation of neighboring bridge sites due to high oxygen coverage. This is expressed in the In–O–In bond angle, which is 157 deg for *Y* but 100–115 deg for all other topologies. We confirmed this by calculating the *Y* configuration with every other bridge site left vacant (0.5 ML coverage), which decreased the In–O–In bond angle to 113° deg and brought the formation energy per oxygen down to  $-2.70$  and  $+0.66$  eV with respect to the  $O_2$  and  $H_2/H_2O$  references, respectively. These values make *Y* competitive with the other configurations listed in Table 1.

Although our results do not represent an exhaustive configurational search, they suggest that any real oxide should consist of In–O–In and In–O–P local bridge morphologies. Indeed, experimental studies of surface oxides on InP(001) have confirmed this to be the case,<sup>23</sup> validating our models.

**Table 1** Energies of relaxed oxygen-rich surface structures (electron volts per oxygen) relative to the reference state (see text for details). Symmetry site for initial oxygen placement is also listed, along with the final location of the oxygen with respect to the top indium layer (surface or subsurface) and the oxygen bond topology (In–O–In bridging versus In–O–P bridging). Compare to Fig. 3.

Initial site	Energy (O <sub>2</sub> ref.)	Energy (H <sub>2</sub> /H <sub>2</sub> O ref.)	Percent In–O–In (%)	Percent In–O–P (%)	Notation in text
Atop	−2.47	+0.89	50	50	<i>A1</i>
Atop	−2.51	+0.85	75	25	<i>A2</i>
Atop	−2.56	+0.80	75	25	<i>A3</i>
Bridge <i>x</i>	−3.02	+0.34	0	100	<i>X</i>
Bridge <i>y</i>	−1.97	+1.39	100	0	<i>Y</i>
Hollow	−2.55	+0.81	0	100	<i>H1</i>
Hollow	−2.70	+0.66	0	100	<i>H2</i>

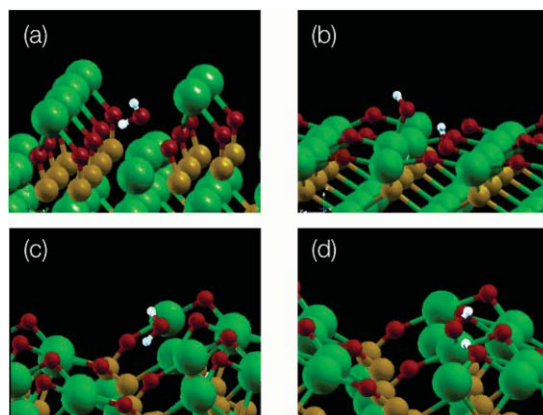


**Fig. 4** Relaxed structure of a single gas-phase water molecule adsorbed on three different oxygen-rich InP(001) surface structures. For the X configuration (a), which features exclusively In–O–P bond topologies, the water molecule remains intact. For the Y configuration (b), which features exclusively In–O–In bond topologies, water dissociation occurs, resulting in local surface hydroxylation. For the A1 configuration (c, d), which features both In–O–In and half In–O–P topologies, water dissociation does not occur if adsorption happens near the In–O–P bond (c), but does occur if adsorption happens near the In–O–In bond (d). Labeling of atomic species follows Fig. 3, with H atoms shown in white.

To test whether surface oxygen affects reactivity for water dissociation, single water molecules were adsorbed near the oxygen sites on the morphologies in Table 1. In each case, oxygen bond topology proves an excellent predictor of gas-phase dissociative adsorption of water: oxygen sites in In–O–P bonds bind water weakly and do not encourage dissociation, whereas sites in In–O–In bonds promote barrierless spontaneous dissociative adsorption. For morphologies containing both types of oxygen bonds, reactivity depends on the specific adsorption site. To illustrate this point, the relaxed configurations for water adsorption on three representative oxygen-rich surfaces (X, Y, A1) are shown in Fig. 4. For the reactive In–O–In topologies, adsorption of water results in cleavage of one of the O–H bonds. The lone hydrogen attaches to one of the surface In–O–In bridging oxygens, whereas the remaining OH moiety attaches to a nearby In atom [Fig. 4(b) and 4(c)]. The result is local surface hydroxylation, suggesting a thermodynamic preference of the system towards hydroxide formation.

#### 4 Structure of Hydroxyl-Rich of Indium Phosphide (001)

In order to investigate the surface structures for hydroxyl-decorated InP(001), we repeated the procedure of placing OH in high-symmetry sites to obtain the relaxed local-minimum structure. In contrast to the rich array of oxygen-decorated surfaces in Table 1, only three unique relaxed configurations were found for OH coverage (bridge y, hollow, and atop). These are shown in Fig. 5. The corresponding energies are listed in Table 2, calculated with respect to the same two references as before: first,  $O_2/H_2$ ; and second,  $H_2/H_2O$ . Again, we used the  $\delta(2 \times 4)$

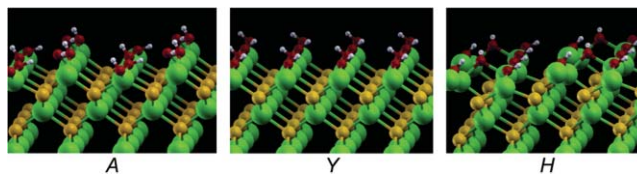


**Fig. 5** Relaxed structures for the hydroxylated surfaces listed in Table 2. Views are along the  $[\bar{1}10]$  crystallographic direction. Labeling of atomic species follows Fig. 3, with H atoms shown in white.

**Table 2** Energies of relaxed hydroxylated surface structures (electron volts per OH) relative to the reference state (see text for details). Compare to Fig. 5.

Initial site	Energy (H <sub>2</sub> /O <sub>2</sub> ref.)	Energy (H <sub>2</sub> /H <sub>2</sub> O ref.)	Notation in text
Atop	−3.63	−0.27	<i>A</i>
Bridge <i>y</i>	−3.69	−0.33	<i>Y</i>
Hollow	−3.63	−0.27	<i>H</i>

reconstruction as the reference configuration for InP(001). We adopt the same notation as for the oxygen-rich surfaces, where *A*=atop, *Y*=bridge *y*, and *H*=hollow indicate the initial hydroxyl adsorption sites.

The three structures in Fig. 5 are very similar, each featuring bridge *y*-derived In–OH–In motifs with variations on the bonding of the remaining OH groups. Notably, unlike the oxygen-decorated case, there are no stable structures featuring an O–P bond. Nevertheless, three distinct local bond configurations for the OH group can be derived from the structures we found. The first, represented in all three structures, is an In–OH–In bridge oriented along  $[\bar{1}10]$  ( $\hat{y}$ ). The second, found in one-quarter of the OH groups for the *H* configuration, is an In–OH–In bridge oriented along  $[110]$  ( $\hat{x}$ ). The third, found in half of the OH groups for the *A* configuration, is a local hydrogen-bond bridge structure oriented along  $[\bar{1}10]$  ( $\hat{y}$ ), featuring paired atop-site dangling OH groups, one of which acts as a hydrogen-bond donor for the other. Each of these three local bond types is similar in strength, as reflected in the near degeneracy of the energies in Table 2. The strength of one of the In–OH bonds in an In–OH–In complex must therefore be competitive with the OH···OH hydrogen bond found in *A*. This implies that immersion in liquid water could facilitate interconversion between the structures in Fig. 5, because the interfacial water should act as a surface hydrogen-bond donor with an energy that competes with In–OH secondary bond formation.

Unlike the oxygen-rich surfaces, Table 2 shows that hydroxylation formation is thermodynamically favored both with respect to the molecular H<sub>2</sub>/O<sub>2</sub> reference and the H<sub>2</sub>O/H<sub>2</sub> reference. This means hydroxylation should be favored in solution as well as under atmospheric conditions. The relative stability of the values in Table 2 over those in Table 1 also confirms the thermodynamic driving force for the dissociation of water on the reactive oxygen-decorated surfaces.

## 5 Molecular Dynamics

Although zero-temperature interactions of III–V semiconductor surfaces with gas-phase water molecules can illustrate some of the local mechanisms that operate at the water–semiconductor interface, the complex dynamics of the surface morphology casts doubt on the transferability of these results to more realistic operating conditions. Accordingly, we have supplemented our zero-temperature results with *ab initio* molecular-dynamics simulations of the full water–semiconductor interface.

We have run three dynamics simulations using model configurations derived from our zero-temperature study. For the oxygen-rich surface, we isolated the In–O–In and In–O–P oxygen bond topologies and examined them in two separate simulations using the *X* configuration (exclusively In–O–P bonds) and the *Y* configuration (exclusively In–O–In bonds). For the hydroxylated surface, we ran only one simulation based on the *Y* configuration, recognizing that the shallow free-energy surface should mean realization of the other morphologies in the course of the dynamics.

### 5.1 Oxygen-Rich Surface

Consistent with our zero-temperature study, the In–O–In bond topology (*Y*) demonstrated much higher reactivity than the In–O–P topology (*X*), with spontaneous water dissociation events

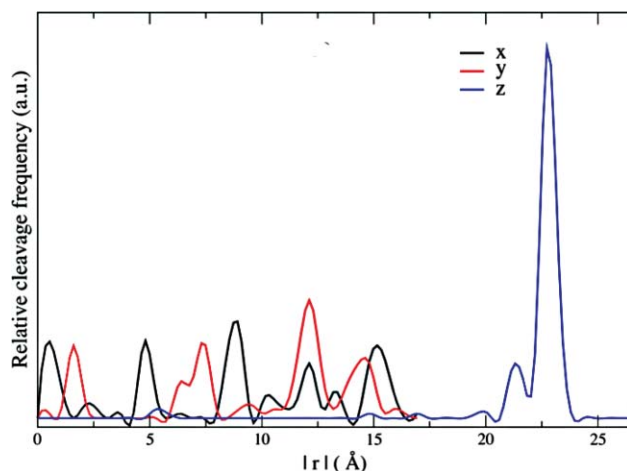


**Fig. 6** Profile of frequency of O–H bond cleavage in water versus location, as projected along the Cartesian axes ( $x$  and  $y$  correspond to the  $[110]$  and  $[\bar{1}10]$  crystal axes, respectively). Data are for InP(001) with the oxygen-rich  $Y$  surface (see Fig. 3). Peaks are normalized against the total number of water-splitting events. The solid surface layer begins at  $z = +25$  Å.

occurring frequently in the former case but not at all in the latter. Figure 6 provides a spatial map of the relative statistical likelihood of water cleavage for the  $Y$  configuration, projected along the  $[110]$  ( $\hat{x}$ ),  $[\bar{1}10]$  ( $\hat{y}$ ), and  $[001]$  ( $\hat{z}$ ) directions. The periodicity of the underlying lattice is clearly visible, and it is easy to see that the reaction takes place near the interface. Along  $\hat{z}$ , two strong peaks are discernible, representing the first and second interfacial water layers. Both are involved in water splitting, although the first surface layer (where the oxygen is adsorbed) is dominant. A small third peak is also present, but its contribution is weak. The existence of non-negligible water-splitting activity as far as 4–5 Å from the actual surface reflects of the medium-range order of liquid water and suggests a dynamical correlation with molecules closer to the interface.

The mechanism of dissociative water adsorption on the reactive oxygen-rich  $Y$  surface, as determined in the molecular-dynamics simulations, is depicted in Figs. 7(a)–7(d). The reaction

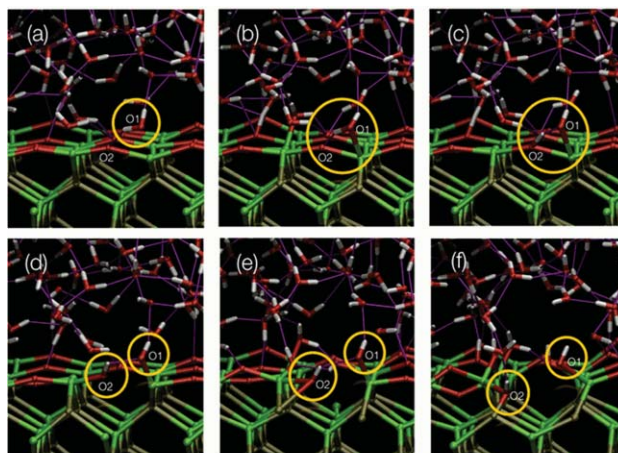


**Fig. 7** Mechanism of water dissociation on the oxygen-rich  $Y$  configuration of InP(001). O1 and O2 refer to the oxygen atoms originally associated with the water molecule and the surface, respectively. (a, b) O1 binds to indium, and a hydrogen bond is formed with O2. (c) The water molecule transfers a hydrogen across the O1–H...O2 complex. (d) The In–O2 bond breaks. (e, f) Optionally, O2 is pulled below the surface to form a bond with P. Labeling of atomic species follows Fig. 3, with H atoms in white.

begins with the adsorption of a water molecule on a surface indium site to form a bond between the water oxygen (O1) and the indium. The water molecule is initially oriented such that one of the O1–H bonds lies generally parallel to the surface, with the other pointing upward into the solution. The parallel-lying O1–H bond is thereby free to engage in hydrogen bonding with one of the surface oxygens (O2). The subsequent cleavage occurs via proton transfer across the O1–H···O2 complex, such that the covalent and hydrogen bonds are exchanged. The result is the hydroxylation of two neighboring indium atoms, the first of which (the one to which the water O1 was originally bound) forms an atop hydroxyl, and the second of which forms either an In–OH atop or In–OH–In bridge hydroxyl.

For most water cleavage events, the reaction culminates in two surface hydroxyl groups (O1–H and O2–H), as in Fig. 7(d). However, there are also instances in which O2 binds to a second-layer phosphorous and is pulled into the subsurface. This phenomenon is depicted in Figs. 7(e) and 7(f). The exact consequences of such hydroxyl incorporation are unclear, although further deprotonation would lead to surface passivation, since the In–O–P configuration is inert to water splitting.

In summary, we observe a competition among three possibilities for the water-splitting by-product hydroxyl groups: first, formation of a In–OH–In bridge; second, formation of an atop OH; and third, incorporation of the OH below the InP(001) surface, where it forms a bridge between In and P. It is worthwhile investigating which local chemical environments preferentially bias the system toward one of the three. Qualitatively, we can conclude that the final configurations of the hydroxyl groups is a function of the local chemical environment, which consists of two primary factors: the number and strength of the hydrogen bonds formed with neighboring water molecules and the occupancy of nearby oxygen bridge sites.

To be pulled into the subsurface, the product oxygen must not be engaged in significant hydrogen bonding. On the other hand, to be converted into the atop hydroxyl configuration, a product oxygen must be engaged in very strong hydrogen bonding. The surface In–OH–In bridge configuration lies intermediate between the two. However, the preexistence of a In–O–In or In–OH–In bridge structure next to the active site precludes formation of another bridge. This has the effect of pushing the system toward one of the other two possibilities. In addition, atop In–OH configurations tend to form on a host In atom that is bound to one other oxygen in a bridge In–O–In topology. This likely alleviates some of the strain induced by coexistence of neighboring oxygen bridges, as discussed above.

## 5.2 Hydroxyl-Rich Surface

Although we start the simulation with all hydroxyl groups in the *Y* configuration (see Fig. 5), a number of these convert to the atop configuration within the first few picoseconds, consistent with the zero-temperature predictions of facile exchange between the two. Following equilibration, the system adopts a dominant but fluctuating pattern of local hydroxyl topologies. This pattern is characterized by preferential breaking of In–OH bonds so as to have an In atom simultaneously bound to only one atop and one bridge OH group. This often results in atop OH groups attached to two neighboring In atoms, which allows one to act as a hydrogen-bond donor for the other, as in the *A* hydroxyl configuration of Fig. 5. The hydrogen bonding serves to stabilize this construction, as does the dissipation of strain energy associated with simultaneous occupation of neighboring In–OH–In bridges, in which degrees of freedom are restricted and a fixed In–In distance is forced.

The hydroxyl-decorated surface shows high affinity for water adsorption. Water molecules are adsorbed exclusively on indium sites, as for the oxygen-decorated surface. In addition, water preferentially adsorbs on indium atoms that are bound to a single oxygen rather than to two oxygens, because this leaves an available binding site. Notably, this undercoordination of indium atoms is connected to conversion of a In–OH–In bridge to an In–OH atop hydroxyl

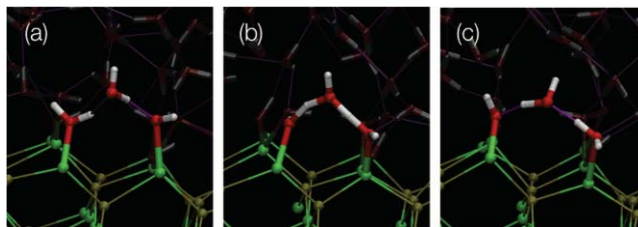


**Fig. 8** Proton transfer across a Grotthuss chain involving an adsorbed water molecule, a water molecule in solution, and an atop OH group. Frames are taken from a molecular-dynamics simulation of the hydroxylated Y configuration of InP(001). The color scheme follows Fig. 4.

configuration. In this way, the local bond topology of hydroxyl-rich surface regions impacts the strength of the interfacial interaction with the first water layer.

We have discussed the hydrogen-bond donor-acceptor pair structure of neighboring surface-adsorbed atop OH groups. An adsorbed water molecule next to an atop OH group can also act as a hydrogen-bond donor, forming a similarly stable complex. In this case, the hydrogen is shared equally between the water molecule donor and the OH acceptor, forming a  $\text{HO}\cdots\text{H}\cdots\text{OH}$  complex in which each oxygen is bound to a surface indium atom. In this case, the O–H bond distance for the shared hydrogen is 1.21 Å, compared to 0.98 Å for an ordinary O–H bond.

Alternatively, the hydrogen-bonded  $\text{H}_2\text{O}\cdots\text{OH}$  complex may involve a second water molecule in the first solution layer. This forms a three-member network chain that echoes the hexagonal symmetry of the underlying lattice. Here, the hydrogens are not shared equally, but the barrier for Grotthuss-type proton transfer across the chain to the adsorbed OH group is lowered. This mechanism for proton exchange, shown in Fig. 8, is commonly observed in the dynamics simulation. Notably, a very similar structure to that of Fig. 8(a) has also appeared in calculations of water on  $\text{TiO}_2$ ,<sup>28</sup> suggesting a link between oxygen-rich InP(001) and conventional oxide surfaces.

## 6 Summary and Conclusions

In summary, we have performed extensive total-energy calculations and *ab initio* molecular-dynamics simulations of water interactions with oxygen- and hydroxyl-decorated surfaces of the model semiconductor InP(001). Whereas several unique oxygen-rich surface structures are identified, fewer hydroxyl-rich configurations are found. The oxygen- and hydroxyl-decorated surfaces can be characterized by the dominant local oxygen bond topology.

For the oxygen-decorated surfaces, the oxygen prefers either to bridge two surface indium atoms along the  $[\bar{1}10]$  ( $\hat{y}$ ) crystallographic direction, or else it bridges a surface indium and subsurface phosphorous. Our *ab initio* molecular-dynamics and total-energy calculations suggest that the In–O–In structure encourages spontaneous dissociation of water at the interface, whereas the In–O–P structure is inactive toward dissociation of water molecules. Additional surface oxygen configurations can be characterized in terms of these two prototypical cases, with dissociative adsorption of water occurring near sites with In–O–In bond topologies and not occurring near sites with In–O–P topologies.

For the hydroxyl-decorated surfaces, the OH group is found either to bridge two surface indium atoms or to bind atop a single indium atom. In the latter case, the dangling OH is likely to be stabilized by a donor-acceptor pair hydrogen bond with a neighboring atop OH or a water molecule in solution. Dynamics on the hydroxylated surfaces demonstrate interconversion between the In–OH–In bridge configuration and the In–OH atop configuration, with indium atoms preferring to bind to one atop OH and one bridge OH simultaneously. Expression of the atop OH configuration enables binding of additional interfacial water, because it occupies only one of the indium binding sites.

Local hydrogen bonding, both between adsorbed surface groups and with the solution, is found to be important in understanding the surface dynamics and reactivity. For the O-decorated surface, hydrogen-bond formation is an important first step in the water splitting reaction. For the OH-decorated surface, hydrogen bonding facilitates rapid surface proton transfer from adsorbed water molecules across Grotthuss network chains. Because the specific hydrogen-bond network topology near the surface fluctuates thermally, our simulations underscore the importance of finite-temperature dynamics in gaining a complete understanding of reactions at the interface. Taken together, our results suggest that oxygen contaminants play an active role in stabilizing transition states and driving dissociative adsorption of water in contact with III-V semiconductor surfaces. In addition, the facile proton transfer within hydrogen-bonded complexes suggests the possibility that proton dynamics may be relevant to the mechanics of hydrogen evolution at the interface.

## Acknowledgments

Funding for this work was provided by the U.S. Department of Energy Fuel Cell Technologies Program. Computing support came from the Lawrence Livermore National Laboratory (LLNL) Institutional Computing Grand Challenge program. This work was performed under the auspices of the U.S. Department of Energy by LLNL under Contract No. DE-AC52-07NA27344.

## References

1. U.S. Department of Energy, “New science for a secure and sustainable energy future,” DOE BESAC Report (2008).
2. A. Fujishima and K. Honda, “Electrochemical photolysis of water at a semiconductor electrode,” *Nature* **238**, 37–38 (1972).
3. N. S. Lewis and D. G. Nocera, “Powering the planet: Chemical challenges in solar energy utilization,” *Proc. Natl. Acad. Sci. USA* **103**, 15729–15735 (2006).
4. J. Turner, G. Sverdrup, M. K. Mann, P.-C. Maness, B. Kroposki, M. Ghirardi, R. J. Evans, and D. Blake, “Renewable hydrogen production,” *Int. J. Energy Res.* **32**, 379–407 (2008).
5. O. Khaselev, J. A. Turner, “A monolithic photovoltaic-photoelectrochemical device for hydrogen production via water splitting,” *Science* **280**, 425–427 (1998).
6. S. Menezes, B. Miller, and K. J. Bachmann, “Electrodissolution and passivation phenomena in III-V semiconducting compounds,” *J. Vac. Sci. Technol. B* **1**, 48–53 (1983).
7. H. J. Lewerenz and K. H. Schulte, “Combined photoelectrochemical conditioning and surface analysis of InP photocathodes: II. photoelectron spectroscopy,” *Electrochem. Acta* **47**, 2639–2651 (2002).
8. J. Vigneron, M. Herlem, E. M. Khoumri, and A. Etcheberry, “Cathodic decomposition of InP studied by XPS,” *Appl. Surf. Sci.* **201**, 51–55 (2002).
9. A. Heller, “Hydrogen-evolving solar cells,” *Science* **223**, 1141–1148 (1984).
10. W. E. Spicer, I. Lindau, P. Skeath, C. Y. Su, and P. Chye, “Unified mechanism for Schottky-barrier formation and III-V oxide interface states,” *Phys. Rev. Lett.* **44**, 420–423 (1980).
11. H. J. Lewerenz, D. E. Aspnes, B. Miller, D. L. Malm, and A. Heller, “Semiconductor interface characterization in photoelectrochemical solar cells: the p-InP (111)A face,” *J. Am. Chem. Soc.* **104**, 3325–3329 (1982).
12. N. Gayathri, S. Izvekov, and G. A. Voth, “*Ab initio* molecular dynamics simulation of the H/InP(100)-water interface,” *J. Chem. Phys.* **117**, 872–884 (2002).
13. A. Heller, B. Miller, H. J. Lewerenz, and K. J. Bachmann, “An efficient photocathode for semiconductor liquid junction cells: 9.4% solar conversion efficiency with p-InP/VCl<sub>3</sub>-VCl<sub>2</sub>-HCl/C,” *J. Am. Chem. Soc.* **102**, 6555–6556 (1980).
14. P. Giannozzi, *et al.*, “QUANTUM ESPRESSO: a modular and open-source software project for quantum simulations of materials,” *J. Phys. Condens. Matter* **21**, 395502 (2009).

15. J. P. Perdew, K. Burke, and M. Ernzerhof, “Generalized gradient approximation made simple,” *Phys. Rev. Lett.* **77**, 3865–3868 (1996).
16. D. Vanderbilt, “Soft self-consistent pseudopotentials in a generalized eigenvalue formalism,” *Phys. Rev. B* **41**, 7892–7895 (1990).
17. R. Car and M. Parrinello, “Unified approach for molecular dynamics and density-functional theory,” *Phys. Rev. Lett.* **55**, 2471–2474 (1985).
18. G. J. Martyna, M. L. Klein, and M. E. Tuckerman, “Nose-Hoover chains: the canonical ensemble via continuous dynamics,” *J. Chem. Phys.* **97**, 2635–2643 (1992).
19. J. C. Grossman, E. Schwegler, E. W. Draeger, F. Gygi, and G. Galli, “Towards an assessment of the accuracy of density functional theory for first principles simulations of water,” *J. Chem. Phys.* **120**, 300–311 (2004).
20. C. W. Wilmsen, “Chemical composition and formation of thermal and anodic oxide/III-V compound semiconductor interfaces,” *J. Vac. Sci. Technol.* **19**, 279–289 (1981).
21. G. Hollinger, E. Bergignat, J. Joseph, and Y. Robach, “On the nature of oxides on InP surfaces,” *J. Vac. Sci. Technol. A* **3**, 2082–2088 (1985).
22. J. Zemek, O. A. Baschenko, M. A. Tyzykhov, and P. Jiricek, “Altered layer composition of sputtered InP(100) wafers: non-destructive concentration depth profiling,” *Surf. Sci.* **318**, 421–427 (1994).
23. G. Chen, S. B. Visbeck, D. C. Law, and R. F. Hicks, “Structure-sensitive oxidation of the indium phosphide (001) surface,” *J. Appl. Phys.* **91**, 9362–9367 (2002).
24. O. Pluchery, Y. J. Chabal, and R. L. Opila, “Wet chemical cleaning of InP surfaces investigated by *in situ* and *ex situ* infrared spectroscopy,” *J. Appl. Phys.* **94**, 2707–2715 (2003).
25. L. Li, Q. Fu, C. H. Li, B.-K. Han, and R. F. Hicks, “Determination of InP(001) surface reconstructions by STM and infrared spectroscopy of adsorbed hydrogen,” *Phys. Rev. B* **61**, 10223–10228 (2000).
26. W. G. Schmidt, “III-V compound semiconductor (001) surfaces,” *Appl. Phys. A* **75**, 89–99 (2002).
27. T. G. Deutsch, C. A. Koval, and J. A. Turner, “III-V nitride epilayers for photoelectrochemical water splitting: GaPN and GaAsPN,” *J. Phys. Chem. B* **110**, 25297–25307 (2006).
28. A. Vittadini, A. Selloni, F. P. Rotzinger, and M. Grätzel, “Structure and energetics of water adsorbed on TiO<sub>2</sub> anatase (101) and (001) surfaces,” *Phys. Rev. Lett.* **81**, 2954–2957 (1998).

Biographies and photographs of the authors not available.